

## Highlights

### **Bayesian Optimisation using microscopic and integral measurements to infer nuclear data parameters**

Daan Houben, Mathieu Hursin, Luca Fiorito, Pierre-Etienne Labeau, Gert Van den Eynde

- Research highlight 1
- Research highlight 2

# Bayesian Optimisation using microscopic and integral measurements to infer nuclear data parameters

Daan Houben<sup>a,b,c</sup>, Mathieu Hursin<sup>c</sup>, Luca Fiorito<sup>a</sup>, Pierre-Etienne Labeau<sup>b</sup>,  
Gert Van den Eynde<sup>a</sup>

<sup>a</sup>*The Belgian Nuclear Research Center (SCK CEN), Boeretang  
190, Mol, 2400, Antwerp, Belgium*

<sup>b</sup>*Université Libre de Bruxelles (ULB), Av. Franklin Roosevelt  
50, Bruxelles, 1050, Bruxelles, Belgium*

<sup>c</sup>*École Polytechnique Fédérale de Lausanne (EPFL), Rte  
Cantonale, Lausanne, 1015, Vaud, Switzerland*

---

## Abstract

Abstract text.

**Keywords:** Nuclear data, MCMC, data assimilation, Chromium

---

## <sup>1</sup> 1. Introduction

<sup>2</sup> Nuclear data is considered the major source of uncertainty in several re-  
<sup>3</sup> actor observables, most notably the effective multiplication factor ( $k_{\text{eff}}$ ). The  
<sup>4</sup> nuclear data available in evaluated nuclear data libraries, such as cross sec-  
<sup>5</sup> tions, neutron multiplicities, angular distributions, and fission neutron energy  
<sup>6</sup> spectra, are the result of a complex fitting procedure involving theoretical  
<sup>7</sup> models, microscopic experiments, and expert judgment. Integral experiments  
<sup>8</sup> are subsequently used to assess the performance of this nuclear data. In this  
<sup>9</sup> work, a Bayesian Optimization (BO) framework is proposed to consolidate

---

*Email address:* daan.houben@sckcen.be (Daan Houben)

<sup>10</sup> microscopic energy-dependent measurements with integral experiments for  
<sup>11</sup> the estimation of nuclear data parameters.

<sup>12</sup> The BO is performed using a Markov Chain Monte Carlo (MCMC) method,  
<sup>13</sup> in which surrogates are employed to evaluate the likelihoods. For the micro-  
<sup>14</sup> scopic energy-dependent measurements, the SAMMY v8.1.0 resonance fit-  
<sup>15</sup> ting tool [1] is employed, while SERPENT v2.2.2 [2], a Monte Carlo neutron  
<sup>16</sup> transport code, is used to quantify the integral response. Surrogates are  
<sup>17</sup> trained by evaluating random samples drawn in the input space using these  
<sup>18</sup> high-fidelity models. The methodology is tested on a case study involving  
<sup>19</sup>  $^{53}\text{Cr}$ . Since microscopic experiments typically provide a dense set of data  
<sup>20</sup> points while integral experiments provide a single values integrated over sev-  
<sup>21</sup> eral nuclides/reactions/energies, special care is taken to analyze how different  
<sup>22</sup> assumptions regarding the likelihood evaluation and data correlation affect  
<sup>23</sup> the posterior distribution.

<sup>24</sup> **2. Background and Mathematical Motivation**

<sup>25</sup> *2.1. Bayesian Optimization Setup*

<sup>26</sup> The main objective of this paper is to infer nuclear data parameter(s) from  
<sup>27</sup> a combined set of microscopic energy-dependent and integral experiments.  
<sup>28</sup> Microscopic energy-dependent measurements (hereafter referred to as micro-  
<sup>29</sup> scopic measurements) quantify single-energy neutron properties. These often  
<sup>30</sup> result from neutron Time-Of-Flight (nTOF) facilities, where the neutron en-  
<sup>31</sup> ergy is derived from the time of flight to a target. A characteristic of these  
<sup>32</sup> measurements is the high density of data points obtained. In contrast, in-  
<sup>33</sup> tegral measurements, such as criticality experiments, provide a single value

<sup>34</sup> representative of a macroscopic group of nuclides, reactions, and energies.

<sup>35</sup> According to Bayes' theorem, the posterior (updated) probability density  
<sup>36</sup> function (PDF),  $P(\theta|\text{data})$ , is proportional to the likelihood of observing the  
<sup>37</sup> parameter(s)  $\theta$  given the data, multiplied by the prior belief regarding the  
<sup>38</sup> parameter(s):

$$P(\theta|\text{data}) \propto P(\text{data}|\theta) \cdot P(\theta) \quad (1)$$

<sup>39</sup> For brevity, we refer to the likelihood as  $\mathcal{L}(\theta) = P(\text{data}|\theta)$ .

<sup>40</sup> *2.2. Markov Chain Monte Carlo (MCMC)*

<sup>41</sup> To calculate the posterior distribution, various techniques derived from  
<sup>42</sup> Bayes' theorem can be employed, such as Generalized Linear Least Squares  
<sup>43</sup> (GLLS) [3], Bayesian Monte Carlo (BMC) [4], and MOCABA [5]. In this  
<sup>44</sup> paper, we select an algorithm belonging to the family of Markov Chain Monte  
<sup>45</sup> Carlo (MCMC) techniques.

<sup>46</sup> In most MCMC algorithms, the unnormalized posterior is evaluated for  
<sup>47</sup> each sample as

$$P^*(\theta|\text{data}) = \mathcal{L}(\theta) \cdot P(\theta), \quad (2)$$

<sup>48</sup> where  $P^*(\theta|\text{data})$  represents the posterior up to a normalizing constant.  
<sup>49</sup> The objective is to construct a Markov chain  $\{\theta_0, \theta_1, \dots, \theta_N\}$  such that the  
<sup>50</sup> stationary distribution of the chain converges to the posterior distribution  
<sup>51</sup>  $P(\theta|\text{data})$ . Under the assumption of a Normally distributed prior ( $\mathcal{N}(\theta_0, \Sigma)$ )  
<sup>52</sup> and likelihood ( $\mathcal{N}(\mathbf{y}_{\text{true}}, \mathbf{A})$ ), the unnormalized posterior probability evalu-

53 stated at  $\theta$  can be rewritten as

$$P^*(\theta|\text{data}) = \frac{1}{\sqrt{(2\pi)^m \det \mathbf{A}}} \exp \left[ -\frac{1}{2} (\mathbf{f}(\theta) - \mathbf{y}_{\text{exp}})^T \mathbf{A}^{-1} (\mathbf{f}(\theta) - \mathbf{y}_{\text{exp}}) \right] \times \\ \frac{1}{\sqrt{(2\pi)^n \det \Sigma}} \exp \left[ -\frac{1}{2} (\theta_0 - \theta)^T \Sigma^{-1} (\theta_0 - \theta) \right] \quad (3)$$

54 The first term represents the probability of observing  $\theta$  given the measurements, where  $\mathbf{y}_{\text{exp}}$  is the vector describing the  $m$  measurement points,  $\mathbf{f}(\theta)$  is the vector containing the model responses for the vector  $\theta$ , and  $\mathbf{A}$  is the covariance matrix describing the measurement points of size ( $m \times m$ ). The prior probability is calculated using the prior belief of the  $n$  parameters  $\theta_0$ , with a covariance matrix  $\Sigma$  of size ( $n \times n$ ).

60 Standard algorithms, such as Metropolis-Hastings, propose a new state  
61  $\theta'$  based on a proposal distribution  $q(\theta'|\theta_t)$  and accept it with probability  
62  $\alpha$ . However, as Metropolis-Hastings algorithms require tuning, we employ  
63 the Affine Invariant Ensemble Sampler (AIES), as implemented in the *emcee*  
64 code [6]. In this algorithm, an ensemble of  $K$  "walkers" is propagated in  
65 parallel. The proposal step for a walker  $\theta_k$  is based on the current position  
66 of a complementary walker  $\theta_j$  from the ensemble:

$$\theta'_k = \theta_j + Z(\theta_k - \theta_j) \quad (4)$$

67 where  $Z$  is a scaling variable drawn from a distribution  $g(z) \propto 1/\sqrt{z}$  on the  
68 interval  $[1/a, a]$ . This "stretch move" allows the algorithm to efficiently sample  
69 distributions with strong correlations without requiring manual tuning of  
70 the proposal covariance matrix.

71    2.3. Likelihood Formulation

72    The formulation of the likelihood function  $\mathcal{L}(\theta)$  is one of the challenges  
 73    when combining integral and microscopic data. The quantity of data points  
 74    differs by orders of magnitude, which may dilute the effect of the integral  
 75    measurement. To better understand the extent to which microscopic mea-  
 76    surements might dilute these integral measurements, we analyze different  
 77    approaches to include the microscopic experiments.

78    Ideally, one would use the full experimental covariance matrix. However,  
 79    calculating experimental correlations between distinct integral experiments,  
 80    distinct microscopic, and between microscopic and integral experiments, is  
 81    inherently difficult and time consuming. We therefore currently introduce the  
 82    assumption that there are no correlations between microscopic and integral  
 83    experiments, nor between integral or microscopic experiments from different  
 84    facilities. This allows us to calculate the total likelihood  $\mathcal{L}(\theta)$  for a set of  
 85    microscopic experiments  $J$  and integral experiments  $I$ :

$$\mathcal{L}(\theta) = \prod_{j \in J} \frac{1}{\sqrt{(2\pi)^{m_j} \det \mathbf{A}_j}} \exp \left[ -\frac{1}{2} (\mathbf{f}_j(\theta) - \mathbf{y}_j)^T \mathbf{A}_j^{-1} (\mathbf{f}_j(\theta) - \mathbf{y}_j) \right] \times \\ \prod_{i \in I} \frac{1}{\sqrt{2\pi\sigma_i^2}} \exp \left[ -\frac{(f_i(\theta) - y_i)^2}{2\sigma_i^2} \right] \quad (5)$$

86    Using the log-likelihood  $\ln \mathcal{L}(\theta)$  for numerical stability:

$$\ln \mathcal{L}(\theta) = -\frac{1}{2} \sum_{j \in J} \ln [(2\pi)^{m_j} \det \mathbf{A}_j] - \frac{1}{2} \sum_{j \in J} [(\mathbf{f}_j(\theta) - \mathbf{y}_j)^T \mathbf{A}_j^{-1} (\mathbf{f}_j(\theta) - \mathbf{y}_j)] + \\ -\frac{1}{2} \sum_{i \in I} \ln [2\pi\sigma_i^2] - \frac{1}{2} \sum_{i \in I} \frac{(f_i(\theta) - y_i)^2}{\sigma_i^2} \quad (6)$$

87    We analyze two approximations regarding the microscopic data: (1) all mi-  
 88    croscopic measurement points behave fully independently, and (2) micro-

89 scopic points within a single experiment are fully correlated (correlation co-  
 90 efficient of 1) while remaining independent of other experiments.

91 *2.3.1. Independent microscopic measurement points*

92 If all measurement points are independent, each microscopic point carries  
 93 the same weight as an integral experiment. Consequently, the integral exper-  
 94 iments are likely to be diluted and their influence on the posterior negligible.  
 95 This makes the inference overconfident in the microscopic experiments. The  
 96 log-likelihood from Eq. 6 becomes:

$$\begin{aligned}\ln \mathcal{L}_J(\theta) &= -\frac{1}{2} \sum_{j \in J} \sum_{e \in E_j} \ln [2\pi\sigma_{j,e}^2] - \frac{1}{2} \sum_{j \in J} \sum_{e \in E_j} \left[ \frac{(f_{j,e}(\theta) - y_{j,e})^2}{\sigma_{j,e}^2} \right] \\ &= C - \frac{1}{2} \sum_{j \in J} \chi_j^2\end{aligned}\quad (7)$$

97 where  $\chi^2$  is the standard goodness-of-fit. The logarithmic term is constant  
 98 with respect to  $\theta$  and is replaced by  $C$ .

99 *2.3.2. Fully correlated microscopic measurement points*

100 Conversely, if we assume microscopic points are fully correlated, we nor-  
 101 malize by the degrees of freedom ( $N$ ), which may be interpreted as taking  
 102 the average. Eq. 6 then becomes

$$\begin{aligned}\ln \mathcal{L}_J(\theta) &= -\frac{1}{2} \sum_{j \in J} \frac{1}{N} \sum_{e \in E_j} \ln [2\pi\sigma_{j,e}^2] - \frac{1}{2} \sum_{j \in J} \frac{1}{N} \sum_{e \in E_j} \left[ \frac{(f_{j,e}(\theta) - y_{j,e})^2}{\sigma_{j,e}^2} \right] \\ &= C - \frac{1}{2} \sum_{j \in J} \chi_{N,j}^2,\end{aligned}\quad (8)$$

103 where  $\chi_{N,j}^2$  is the chi-squared per degree of freedom for microscopic exper-  
 104 iment  $j$ . In this approximation, we are too conservative and do not trust

105 the microscopic experiment sufficiently. Eventually, including the full exper-  
106 imental covariance matrix will result in a likelihood which is inbetween the  
107 result obtained by Eqs. 7 and 8.

108 *2.4. Surrogate Modelling*

109 The MCMC algorithm requires thousands of likelihood evaluations. Di-  
110 rectly executing high-fidelity codes (SAMMY and SERPENT) at each step  
111 is computationally expensive. We therefore employ Gaussian Process (GP)  
112 regression as a surrogate model. A GP defines a probability distribution  
113 over all possible functions consistent with the observed data, providing both  
114 a predicted mean and an associated variance. This variance can then be in-  
115 cluded in the likelihood calculation and allows the MCMC sampler to avoid  
116 overconfidence in less explored regions of the input space.

117 To train the surrogates, a dataset is generated by drawing uniform ran-  
118 dom samples across the input space. For microscopic experiments, SAMMY  
119 calculates the  $\chi^2$  metric. For integral experiments, SERPENT calculates  $k_{\text{eff}}$ .  
120 The dataset is split 80/20 for training and testing. We utilize a Radial Basis  
121 Function (RBF) kernel for the integral experiments (as  $k_{\text{eff}}$  behaves smoothly)  
122 and a polynomial kernel of second degree for the microscopic  $\chi^2$  response (as  
123  $\chi^2$  is inherently quadratic). A white noise kernel is added to account for  
124 Monte Carlo statistical uncertainty and to ensure positive definiteness.

125 *2.5. Including Uncertainties of Other Nuclides*

126 To limit the Bayesian Optimization from compensating for biases induced  
127 by other sources, next to the uncertainties introduced by material and geom-  
128 etry specifications, uncertainties from other nuclides should also be included.

129 For criticality experiments, we estimate these using relative first-order sensi-  
130 tivity coefficients  $S_{k,\sigma} = \frac{\partial k/k}{\partial \sigma \sigma}$  calculated via Generalized Perturbation Theory  
131 (GPT) as implemented in SERPENT-2 using the ECCO-33 multi-group en-  
132 ergy structure [7].

133 Covariance matrices  $\Sigma_\sigma$  were generated using SANDY [8] (wrapping NJOY2016 [9]).  
134 The Sandwich formula [10] is used to propagate these uncertainties to  $k_{\text{eff}}$ , it  
135 is given by

$$\Sigma_k = S_{k,\sigma}^T \cdot \Sigma_\sigma \cdot S_{k,\sigma}, \quad (9)$$

136 where  $\Sigma_k$  is the covariance matrix describing  $k_{\text{eff}}$  of the systems under con-  
137 sideration and  $S_{k,\sigma}$ , the matrix containing the sensitivity vectors of each sys-  
138 tem, is the relative first-order sensitivity coefficients describing how changes  
139 in nuclear data affect  $k_{\text{eff}}$ . These nuclear data variances are then added to the  
140 experimental variance. This ensures the adjustment does not falsely correct  
141 for other nuclear data biases. As a consequence, the integral experiments  
142 (mostly criticality) become less informative, as they are heavily influenced  
143 by uncertainties due to fissile nuclides.

### 144 3. Description of Cases

#### 145 3.1. Chromium-53

146 Chromium is a frequently used structural element in nuclear reactors,  
147 here 11-26% of chromium is added to stainless steel in order to increase  
148 its corrosion resistance. Due to the scattering and capture cross sections  
149 in  $^{50}\text{Cr}$ ,  $^{52}\text{Cr}$  and  $^{53}\text{Cr}$ , it is also important for criticality safety in some  
150 nuclear systems [11]. A major isotope with relatively poor nuclear data is  
151 the 1-10 keV range of  $^{53}\text{Cr}$ . Existing microscopic measurements, such as

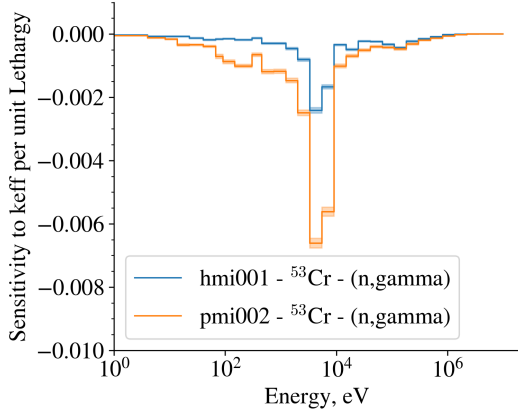


Figure 1: Sensitivity profiles for two criticality experiments sensitive to Cr-53 ( $n,\gamma$ )

152 those by Guber (2011) [12] and Stieglitz (1971) [13], are not consistent with  
 153 each other. Recently, Pérez-Maroto et al. (2025) performed new capture  
 154 yield measurements, it is seen as a possibility to include this experiment and  
 155 complement it with integral experiments to test the proposed methodology.

156 To start, we selected two criticality experiments, i.e., PMI-002 and HMI-  
 157 001, due to their significant sensitivity in the 1-10 keV range (see Figure 1).  
 158 These experiments use stainless steel as reflector in an intermediate spectrum.  
 159 They are available in the International Handbook of Evaluated Criticality  
 160 Safety Benchmark Experiments (ICSBEP) [14].

161 For this case study, we infer only the capture width  $\Gamma_\gamma$  at 4 keV, as it is  
 162 the parameter most sensitive to criticality in this range.  $E_r$  and  $\Gamma_n$  are not  
 163 perturbed as they are more easily derived from transmission measurements.  
 164 This serves as a simplified proof-of-concept and an extension to multiple  
 165 input parameters is possible. The perturbation of  $\Gamma_\gamma$  is shown in Figure  
 166 2. Here, the capture yield (a) represents the connection to the microscopic  
 167 measurements performed by Pérez-Maroto et al., while (b) represents the

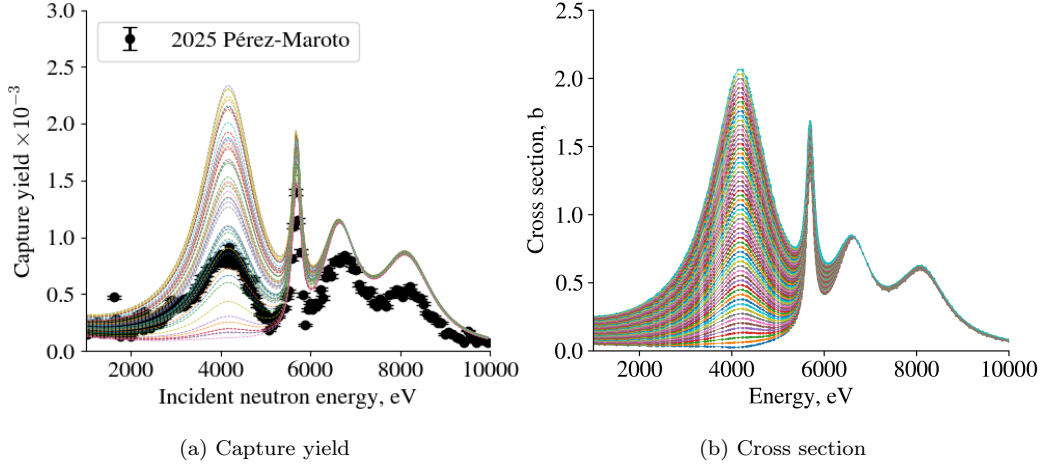


Figure 2: Random samples for capture yield (A) and cross section (B).

<sup>168</sup> cross sections which have been incorporated into ACE files, ready for use in  
<sup>169</sup> the SERPENT-2 Monte Carlo code. For each of these curves, the SAMMY  
<sup>170</sup> and SERPENT codes were run with the goal of training a surrogate GP.

#### <sup>171</sup> 4. Results and Discussions

##### <sup>172</sup> 4.1. Chromium-53

<sup>173</sup> The validation of the Gaussian Process is shown in Figure 3, in (a) the  
<sup>174</sup> data points and the GP for the Pérez-Maroto data set is shown, while in  
<sup>175</sup> (b) it is shown for PMI-002. The GP corresponds well with the predicted  
<sup>176</sup> responses obtained from SAMMY and SERPENT, obviously since they were  
<sup>177</sup> trained on them. Nevertheless, the tests performed on the 20% of data points  
<sup>178</sup> which were not included in the assimilation were also in good agreement with  
<sup>179</sup> the GP prediction.

<sup>180</sup> We analyze several scenarios: integral experiments only, microscopic ex-  
<sup>181</sup> periments only, and combinations using the independent vs. fully correlated

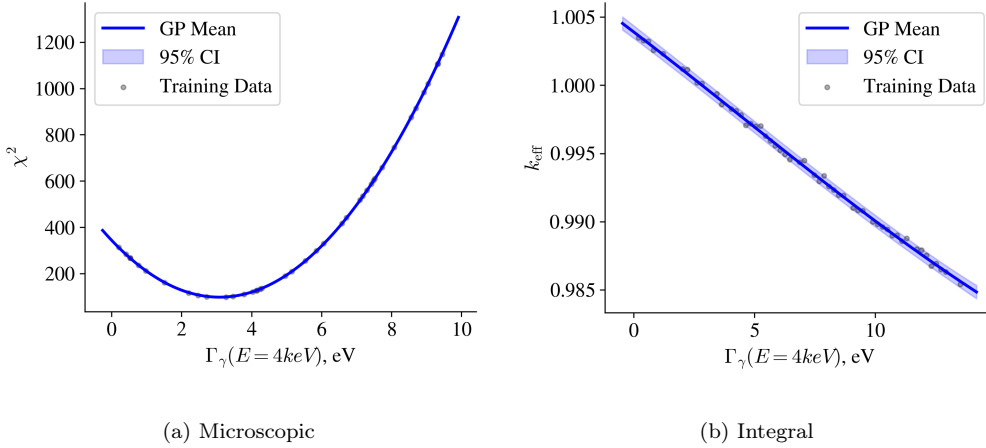


Figure 3: GPs for microscopic (a) and integral (b) experiment.

assumptions. The results are summarized in Table 1.

To confine the effect of including some experiments, various scenarios are simulated. In case 1, to experiments are included, which corresponds to the prior input parameters taken from JEFF-4.0, but with an increased relative uncertainty to make the prior less informative. Then, as a baseline Eq. 8 is used unless otherwise noted. In case two, both integral experiments are included and the mean shifts only slightly and the posterior uncertainty is also not improved much. This can be attributed to the large uncertainty due to other nuclear data uncertainties in comparison to the rather limited sensitivity to the first  $\Gamma_\gamma$  of  $^{53}\text{Cr}$ . In contrast, when these other nuclear data uncertainties are neglected, as can be seen in case 6, the bias shifts by about 30%, while the uncertainty is reduced by 7%.

Now, the influence of fully correlated and independent microscopic measurement points is compared. In case 3, only the microscopic experiment from Pérez-Maroto is included with the assumption of fully correlated mea-

Table 1: Overview of posterior mean and uncertainty for different combinations of experiments included.

Case	PMI002	HMI001	ntof	$\Gamma_\gamma$ , eV	$\sigma_\Gamma$ (%)	Comment
1				4.14	20	Prior
2	✓	✓		4.16	19.7	
3			✓	3.14	6	
4	✓	✓	✓	3.15	6	Fully correlated
5	✓	✓	✓	3.09	2	Independent
6	✓	✓		5.52	13	No other ND uncertainty
7			✓	3.09	2	Independent

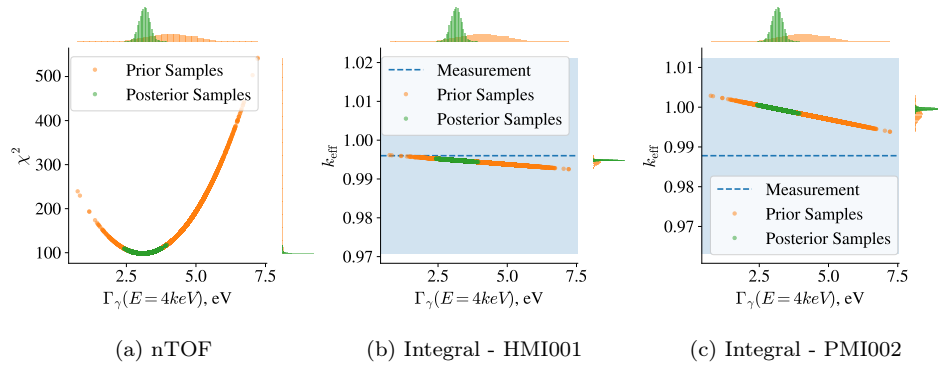


Figure 4: Scatter plots for microscopic (A) and integral (B and C) experiments showing the prior and posterior responses as a function of the input variable for Case 4.

surement points. Then, the posterior is optimized to be consistent with only this measurement and the  $\Gamma_\gamma$  moves down. This is in contradiction with the adjustment proposed by case 6, but cannot be rejected by the posterior in case 2 where the other nuclear data uncertainties are included. The posterior uncertainty is then reduced to 6%. Now, when the assumption of fully independent microscopic data points is used, such as in case 7 or also in Figure 5. Here the posterior seems to be confident in the prediction of  $\Gamma_\gamma$  with a posterior uncertainty of 2%.

In Figure 4, corresponding to case 4 is depicted. Here the two integral experiments PMI-002 and HMI-001 as well as the microscopic dataset (regarded as fully correlated) from Pérez-Maroto are included. The posterior prediction of  $k_{\text{eff}}$  moves away from the calculated integral response for PMI-002, but remains well within the uncertainty bounds imposed by experimental and other nuclear data sources. It appears that the included integral experiments contribute negligibly to the uncertainty reduction in the  $\Gamma_\gamma$  parameter at 4 keV. In order to be able to include integral experiments into this mix, several things are needed. First, the nuclear data uncertainties of other sources should be kept to a minimum, either by experimental design, or by reducing them using data assimilation with integral experiments that are sensitive to the most important other nuclear data uncertainties. Nevertheless, it seems criticality experiments are not sufficiently sensitive to the  $\Gamma_\gamma$ -width of  $^{53}\text{Cr}$  at 4 keV. A possible route to increase the sensitivity is to design experiments specifically sensitive to this energy range, e.g. pile-oscillation experiments with a significant portion of the spectrum in this energy range. On the other hand, nuclides which are more important for  $k_{\text{eff}}$ , such as  $^{238}\text{U}$  /  $^{235}\text{U}$  or  $^{239}\text{Pu}$

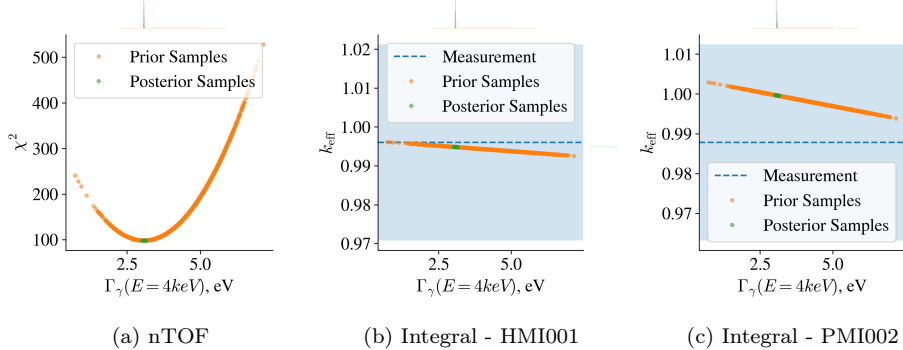


Figure 5: Scatter plots for Case 5 (Independent assumption).

222 might be more suitable candidates for testing as a much larger suite of highly  
223 sensitive integral experiments are available.

224 Finally, we simulate a hypothetical scenario with highly sensitive integral  
225 experiments (experimental uncertainty reduced to 10 pcm and other nuclear  
226 data uncertainties neglected). As seen in Figure 6, under these ideal and  
227 unrealistic conditions, integral experiments provide significant guidance to  
228 the posterior. Although we know the integral experiments are subjected to  
229 larger uncertainties of other nuclides, it shows that when experiments with  
230 a lower uncertainty in comparison to the sensitivity are used, they can be  
231 combined with microscopic experiments under the conservative assumption  
232 that microscopic data points behave as one.

## 233 5. Conclusions and Future Work

234 In this work, a Bayesian Optimization framework was implemented to  
235 infer nuclear data parameters by consolidating microscopic and integral ex-  
236 periments. The methodology coupled SAMMY and SERPENT with Gaus-  
237 sian Process surrogates and an MCMC sampler, allowing for more efficient

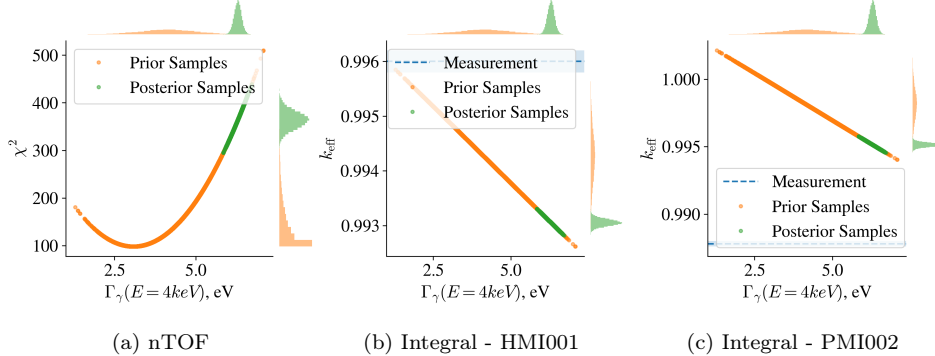


Figure 6: Scatter plots for the hypothetical high-sensitivity scenario.

238 exploration of the posterior distribution.

239 The case study on  $^{53}\text{Cr}$  highlighted the critical challenge of weighting  
 240 different data sources. We demonstrated that the assumption regarding cor-  
 241 relations in microscopic data fundamentally alters the posterior. Treating  
 242 microscopic points as independent results in an overconfident reduction of  
 243 uncertainty in which integral experiments become negligible. On the other  
 244 side, when microscopic data is treated as fully correlated (per experiment)  
 245 and uncertainties for other nuclides are also included, the criticality experi-  
 246 ments currently available for  $^{53}\text{Cr}$  provide negligible information gain. They  
 247 are dominated by the uncertainties due to fissile nuclides.

248 The results indicate that for integral experiments to be valuable in this  
 249 framework, either the experiments must be chosen such that the parameter  
 250 to infer is sufficiently sensitive in comparison to other nuclear data, or the  
 251 uncertainties of other nuclear data must be significantly reduced using a-  
 252 priori data assimilation techniques.

253 Future work should be devoted to including a realistic experimental co-  
 254 variance matrix to assess the validity of the assumptions regarding indepen-

dent / fully correlated data samples. Second, since the case study on  $^{53}\text{Cr}$  did not yield significant results, the framework could be applied to a realistic scenario involving for example  $^{238}\text{U}$ , where many highly sensitive integral experiments are available. Some points that still should be addressed include implementing correlations between experiments and including the GP prediction uncertainty in the loglikelihood of the microscopic experiment. Although the latter is not expected to influence the results since SAMMY is deterministic, therefore the prediction uncertainty attributed to the GP response is negligible.

## 6. Acknowledgments

The authors gratefully acknowledge the financial support of the Fonds de la Recherche Scientifique (F.R.S.-FNRS) and the ENEN2plus project. The ENEN2plus project has received funding from the Euratom research and training programme 2021-2025 under grant agreement No 101061677. The authors also like to thank Sara Maccario for providing a set of scripts which helped speed up development. Finally, we thank Peter Schillebeeckx for the insightful discussions. At last, the help of Pablo Pérez-Maroto is also greatly appreciated for providing input files for SAMMY.

## References

- [1] N. M. Larson, Updated User's Guide for Sammy: Multilevel R-Matrix Fits to Neutron Data Using Bayes' Equations. doi:10.2172/941054.  
URL <http://www.osti.gov/servlets/purl/941054-BqQIH/>

- 277 [2] J. Leppänen, M. Pusa, T. Viitanen, V. Valtavirta, T. Kaltiaisenaho,  
278 The Serpent Monte Carlo code: Status, development and applications  
279 in 2013, Annals of Nuclear Energy 82 (2015) 142–150. doi:10.1016/j.  
280 anucene.2014.08.024.
- 281 [3] A. Hoefer, O. Buss, J. C. Neuber, Limitations of the Generalized Linear  
282 Least Squares Methodology for Bias Estimation in Criticality Safety  
283 Analysis.
- 284 [4] D. Rochman, E. Bauge, A. Vasiliev, H. Ferroukhi, S. Pelloni, A. J.  
285 Koning, J. Ch. Sublet, Monte Carlo nuclear data adjustment via integral  
286 information, The European Physical Journal Plus 133 (12) (2018) 537.  
287 doi:10.1140/epjp/i2018-12361-x.
- 288 [5] A. Hoefer, O. Buss, M. Hennebach, M. Schmid, D. Porsch, MOCABA:  
289 A general Monte Carlo–Bayes procedure for improved predictions of  
290 integral functions of nuclear data, Annals of Nuclear Energy 77 (2015)  
291 514–521. doi:10.1016/j.anucene.2014.11.038.
- 292 [6] D. Foreman-Mackey, D. W. Hogg, D. Lang, J. Goodman, emcee: The  
293 mcmc hammer, Publications of the Astronomical Society of the Pacific  
294 125 (925) (2013) 306–312. doi:10.1086/670067.  
295 URL <http://dx.doi.org/10.1086/670067>
- 296 [7] M. Aufiero, A. Bidaud, M. Hursin, J. Leppänen, G. Palmiotti,  
297 S. Pelloni, P. Rubiolo, A collision history-based approach to sensitiv-  
298 ity/perturbation calculations in the continuous energy Monte Carlo

- 299 code SERPENT, Annals of Nuclear Energy 85 (2015) 245–258. doi:  
300 [10.1016/j.anucene.2015.05.008](https://doi.org/10.1016/j.anucene.2015.05.008).
- 301 [8] L. Fiorito, J. Dyrda, M. Fleming, JEFF-3.3 covariance application to  
302 ICSBEP using SANDY and NDAST, EPJ Web of Conferences 211  
303 (2019) 07003. doi:[10.1051/epjconf/201921107003](https://doi.org/10.1051/epjconf/201921107003).
- 304 [9] D. W. Muir, R. M. Boicourt, A. C. Kahler, J. L. Conlin, W. Haeck, The  
305 NJOY Nuclear Data Processing System, Version 2016.
- 306 [10] B. L. Broadhead, B. T. Rearden, C. M. Hopper, J. J. Wagschal, C. V.  
307 Parks, Sensitivity- and Uncertainty-Based Criticality Safety Validation  
308 Techniques, Nuclear Science and Engineering 146 (3) (2004) 340–366.  
309 doi:[10.13182/NSE03-2](https://doi.org/10.13182/NSE03-2).
- 310 [11] A. Trkov, O. Cabellos, R. Capote, Sensitivity of selected benchmarks to  
311 Cr-53 and Cr-50 capture.
- 312 [12] K. H. Guber, P. E. Koehler, D. E. Wiarda, J. A. Harvey, Neutron Cross-  
313 Section Measurements on Structural Materials at ORELA, Journal of  
314 the Korean Physical Society 59 (2(3)) (2011) 1685–1688. doi:[10.3938/jkps.59.1685](https://doi.org/10.3938/jkps.59.1685).
- 316 [13] R. Stieglitz, R. Hockenbury, R. Block, kev neutron capture and trans-  
317 mission measurements on 50cr, 52cr, 53cr, 54cr, 60ni and v, Nuclear  
318 Physics A 163 (2) (1971) 592–624.
- 319 [14] International Criticality Safety Benchmark Evaluation Project (ICS-  
320 BEP), International Handbook of Evaluated Criticality Safety Bench-  
321 mark Experiments, OECD Nuclear Energy Agency (NEA), 2024.